

## Characterization of a vertically aligned silica nanospring-based sensor by alternating current impedance spectroscopy

This article has been downloaded from IOPscience. Please scroll down to see the full text article.

2010 J. Micromech. Microeng. 20 095005

(<http://iopscience.iop.org/0960-1317/20/9/095005>)

View [the table of contents for this issue](#), or go to the [journal homepage](#) for more

Download details:

IP Address: 173.50.183.166

The article was downloaded on 11/08/2010 at 23:19

Please note that [terms and conditions apply](#).

# Characterization of a vertically aligned silica nanospring-based sensor by alternating current impedance spectroscopy

Yukta P Timalisina<sup>1</sup>, Dennis Oriero<sup>2</sup>, Timothy Cantrell<sup>3</sup>, Tej Prakash<sup>3</sup>,  
Joshua Branen<sup>1</sup>, D Eric Aston<sup>2</sup>, Kenneth Noren<sup>4</sup>, James J Nagler<sup>5</sup>,  
Shiva Rastogi<sup>6</sup>, David N McIlroy<sup>1</sup> and Giancarlo Corti<sup>1,3,7</sup>

<sup>1</sup> Department of Physics, University of Idaho, Moscow, ID 83844, USA

<sup>2</sup> Department of Chemical and Materials Engineering, University of Idaho, Moscow, ID 83844, USA

<sup>3</sup> GoNano Technologies Inc., Moscow, ID 83843, USA

<sup>4</sup> Department of Electrical and Computer Engineering, University of Idaho, Moscow, ID 83844, USA

<sup>5</sup> Department of Biological Sciences, University of Idaho, Moscow, ID 83844, USA

<sup>6</sup> BANL, University of Idaho, Coeur d'Alene, ID 83814, USA

E-mail: [corti@gonano-9.com](mailto:corti@gonano-9.com) and [corti@uidaho.edu](mailto:corti@uidaho.edu)

Received 11 March 2010, in final form 5 July 2010

Published 5 August 2010

Online at [stacks.iop.org/JMM/20/095005](http://stacks.iop.org/JMM/20/095005)

## Abstract

In this study, the initial phase of development of a vertically aligned (silica) nanospring (VANS)-based sensor utilizing alternating current impedance spectroscopy is presented. The sensor is a capacitor consisting of two glass substrates coated with indium tin oxide, where the VANS are grown on one substrate, following a top-down approach, serving as the dielectric spacer layer. The sensitivity of the VANS sensors was evaluated using deionized water (of an effective  $\approx 10^{-3}$  mM monovalent ion concentration) and saline-phosphate (SP) solutions of pH 7.3 with concentrations 0.1, 1, 10 and 100 mM. Similar tests were performed with sensors without VANS or blank sensors. The modeling of the VANS impedance spectra required an equivalent circuit consisting of eight elements compared to four elements for the blank sensor. VANS sensors exhibited greater sensitivity to changes in the SP concentration relative to the blank sensors. The enhanced sensitivity is attributed to the addition of an ionic diffusion barrier at the VANS–solution interface and to ionic diffusion within the VANS.

(Some figures in this article are in colour only in the electronic version)

## 1. Introduction

Electrical devices that can be used as sensors continue to attract the interest of academic and corporate research groups around the world [1–3]. With the development of new nanomaterials, the utilization of nanomaterials is growing exponentially [4, 5]. The various classes of nanomaterials are two-dimensional (thin films), one-dimensional (nanowires, nanosprings, etc.) and zero-dimensional (nanoparticles). Silica ( $\text{SiO}_x$ ) nanomaterials are an extremely popular type due to their biocompatibility [6].

Silica nanospring mats [7–11], in particular, have a number of important features that make them a platform for applications in electrical sensing, e.g. surface area. In addition, the large surface-to-volume ratio and the three-dimensional geometry of nanospring mats result in an open pore structure that is readily accessible by large biomolecules compared to mesoporous silica, for example. VANS provide a larger density of nanomaterial per square centimeter compared with standard silica nanosprings.

The objective of our program is to develop VANS-based sensors for electrical-based biodetection, where this study is

<sup>7</sup> Author to whom any correspondence should be addressed.

only the first step in the development of a fully functional VANS biosensor. Many biological systems of interest, such as DNA detection, require a very specific environment, i.e. pH, salt concentration, etc. For example, DNA will denature without suspension in a saline solution. Consequently, an electrical sensor will require the device to operate in a solution compatible with DNA. The motion of the ions in the solution by themselves will produce a response due to an applied electric field. The nonspecific response of the sensor to ionic transport must be well characterized in order to distinguish it from the true signal of interest. Only upon completion of this analysis, can one proceed to the next step of biosensor development. Consequently, we are reporting on the first phase of VANS-based biosensor development: nonselective device response as a function of ionic concentration in a buffer solution.

The proposed operational mode of the sensor is as an alternating current (AC) device, where impedance spectroscopy or electrochemical impedance spectroscopy (EIS) is the detection method. EIS consists of applying a sinusoidal potential (or current, in some cases) to the system and monitoring the amplitude and phase shift of the current (or voltage) response [12–15]. The present work shows a matching of the experimental data with the electrical model to characterize the ionic transport phenomena of the VANS-based biosensor. The provided equivalent electric circuit of the VANS-based biosensor model represents an electrochemical reaction occurring at electrode/solution interfaces. Similar electrical modeling was done for a blank sensor to compare against the VANS sensor.

## 2. Experimental procedures

### 2.1. Device fabrication

The sensor design is a standard parallel plate capacitor with upper and lower electrodes made of indium tin oxide (ITO) and the dielectric, or sensing media, made of VANS surrounded by the test fluid. The micro/nanofabrication procedure shown in figure 1 followed a top-down approach, which simplifies fabrication and nanomaterial handling [10]. The starting substrates were  $25 \times 25$  mm ITO coated glass slides (Delta Technologies) with an average sheet resistance of  $25 \Omega$ . The ITO substrates were coated with a  $6 \mu\text{m}$  photoresist layer (SIPR9740-9) and patterned to produce the rectangular-shaped electrodes. ITO was etched using an ITO etchant (TE-100). The photoresist was removed and the sample cleaned to reveal the finished electrode geometry. Half of the substrates were recoated with the sacrificial  $6 \mu\text{m}$  thick photoresist and patterned with a re-entrant profile for a lift-off process [16].

VANS were grown in the patterned areas of these substrates by GoNano Technologies (Moscow, Idaho). The technology used to grow the nanosprings has been previously reported by Wang *et al* [8] and McIlroy *et al* [11]. Due to the pending application for a US patent [17] on this nanospring technology, only a condensed description of the process will be presented. The nanospring synthesis was performed in

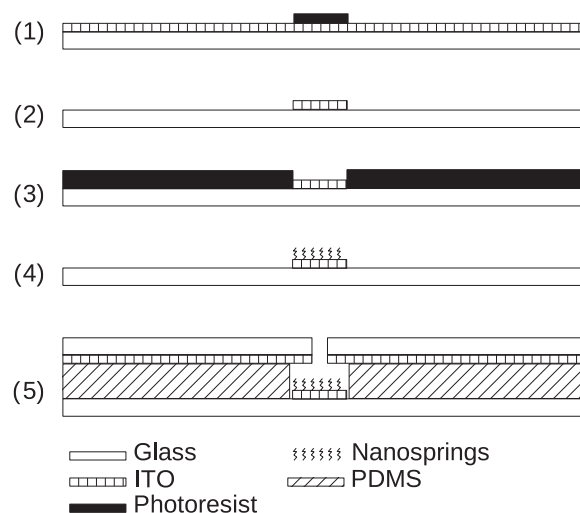


**Figure 1.** A schematic diagram of the micro- and nano-process.

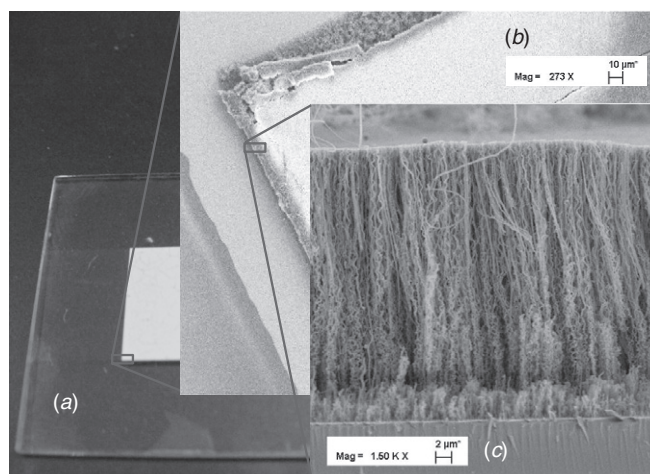


**Figure 2.** (a) Bottom electrode plate with the VANS, (b) close up of the patterned VANS, (c) scanning electron microscopy micrograph of the VANS.

a furnace operated at atmospheric pressure. The general principles of this furnace were discussed in detail by McIlroy *et al* [11]. The process uses a thin gold layer as a catalyst which is then exposed to a proprietary silicon precursor [17]. During VANS synthesis a constant  $\text{O}_2$  flow rate is maintained concomitant with the silicon precursor. With a growth time of 15 min, a  $36.3 \pm 0.11 \mu\text{m}$  thick VANS mat is achieved. The average coil and wire diameters of the VANS are  $113.4 \pm 7 \text{ nm}$  and  $20.9 \pm 1.5 \text{ nm}$ , respectively. Figure 2 shows sequential magnifications of a portion of the final VANS electrode.

Using the remaining patterned blank substrates, i.e. sans VANS, the center of the ITO pad is located, and a 3 mm diameter hole is drilled through them using a diamond bit. These substrates serve as the top electrode. Both electrodes were placed in a jig separated by a  $200 \mu\text{m}$  thick polydimethylsiloxane (PDMS) gasket, as shown in figure 1. Blank sensors were constructed in the same sans VANS.

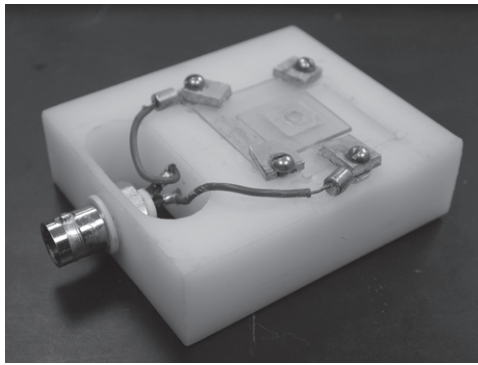


**Figure 3.** A VANS sensor mounted on the test jig.

## 2.2. Test procedure

In this study, five blank and nine VANS sensors were evaluated. The test solutions consisting of deionized water (of an effective  $\approx 10^{-3}$  mM monovalent ion concentration) or saline-phosphate (SP) solutions of pH 7.3 with concentrations of 0.1, 1, 10 and 100 mM were introduced into the VANS sensor, or the blank sensor, via the 3 mm hole in the upper electrode (see figure 3). Potentiostatic measurements were carried out, which consisted of applying a voltage between working electrodes while simultaneously measuring the current flowing between the two electrodes through the solution. A VersaSTAT3 with frequency response analyzer and software was used to measure the spectra from 1 Hz to 1 MHz with sine wave amplitude of 10 mV. An Agilent 4395A Network/Spectrum/Impedance analyzer was used to measure the impedance characteristics from 100 kHz to 500 MHz. The measurements were spliced together in order to span the entire frequency range from 1 Hz to 500 MHz.

The first step of testing was to demonstrate the temporal stability of the VANS sensor, as well as the blank. All of the VANS and the blank sensors were tested over 1 h with a SP solution of pH 7.3. No changes in the response of the VANS sensors, or blank sensors, were observed. In addition to verifying the temporal stability of the VANS and blank sensors, the test also validated the test procedure where measurements were performed with two test setups over an extended period of time, i.e. a finite amount of time was required to swap the test jig between the two test stations.

Each of the five blank and nine VANS sensors were tested separately with deionized water (of an effective  $\approx 10^{-3}$  mM monovalent ion concentration), and 0.1, 1, 10 and 100 mM NaCl concentrations in SP solution in order to determine their response as a function of the electrolyte concentrations. The use of multiple devices ensures that the changes in the electrical properties due to the presence of VANS can be attributed to the VANS, as opposed to variations in electrode manufacturing, device assembly, testing contacts, etc. The measured impedance response versus frequency of the VANS and blank sensors were modeled with a resistor-capacitor-inductor (RCL) circuit methodology. The values of the fitted circuit elements of the equivalent circuits were averaged between multiple devices and their standard deviations were calculated. Furthermore, variability in the

values of the circuit elements attributed to the VANS provides insight into the repeatability of the VANS process.

## 3. Results and discussion

### 3.1. Blank sensor

The frequency-dependent impedance and phase characteristics for blank sensors with various concentrations (0.1, 1, 10 and 100 mM) of the SP solutions are presented in figures 4(a) and (b) respectively. The impedance spectra of the blank sensor in figure 4(a) can be dissected into three distinct regions. The region below 100 Hz is primarily capacitive in nature. The region from 100 Hz to 1 kHz is the transition region from capacitance to resistance dominated. The blank sensor is almost completely resistive between 1 kHz and approximately 20 MHz. The region between 20 and 100 MHz is the transition region from resistance to inductance. In the frequency range between 100 and 300 MHz the blank sensor is inductive. A closer examination of the spectra in figure 4(a) reveals that the impedance decreases by 28% with increasing salt concentrations from 0.1 to 100 mM below 1 kHz, whereas no significant change in impedance is observed above 60 MHz. The impedance spectra for the blank sensor are interpreted with the typical model equivalent circuit shown in figure 5(a) [15, 18–26]. A physical interpretation of the elements of the model equivalent circuit is outlined in figure 5(b). The assignments are consistent with previously reported studies of blank sensors of this type [18, 20–24].

The sensor includes an electric double layer capacitance  $C_{1,b}$  [27–29], solution resistance of the electrolyte  $R_{s,b}$ , inductance  $L$  and capacitance  $C_3$ .  $C_{1,b}$  is formed at the electrode/solution interface and is proportional to the surface area of the electrode and the ion concentration at the interface. Consequently,  $C_{1,b}$  is affected by the changes of the ion concentration of the electrolyte solution.  $R_{s,b}$  results from the finite conductance of ions present in the electrolyte solution.  $L$  is the self-inductance of the circuit, where contributions come from the electrical leads and test equipment.  $C_3$  is due to the parallel plate configuration of the sensor and not specific to the solution under test. Figures 6(a) and (b) show the measured and fitted impedance magnitude and phase plots, respectively, as a function of frequency for a 100 mM concentration of the SP solution. Excellent agreement between the experimental data and the simulated data is obtained with the model equivalent circuit in figure 5(a). However, at frequencies below 500 Hz the equivalent circuit output deviates from the experimental data since theory requires the capacitance phase to go to the ideal value of  $-90^\circ$ , as opposed to the experimental phase of  $-80^\circ$ . The impedance characteristics for other concentrations (0.1, 1 and 10 mM) were fitted with the equivalent circuit in figure 5(a), where the fits are of equally good quality. The experiments were repeated for five blank sensors. The average values of the elements of the equivalent circuit for the blank sensor as a function of SP concentration are summarized in table 1. Note that the lowest concentration of 0.001 mM refers to deionized water as an estimate only of its equivalent ionic strength estimated from conductivity analysis.

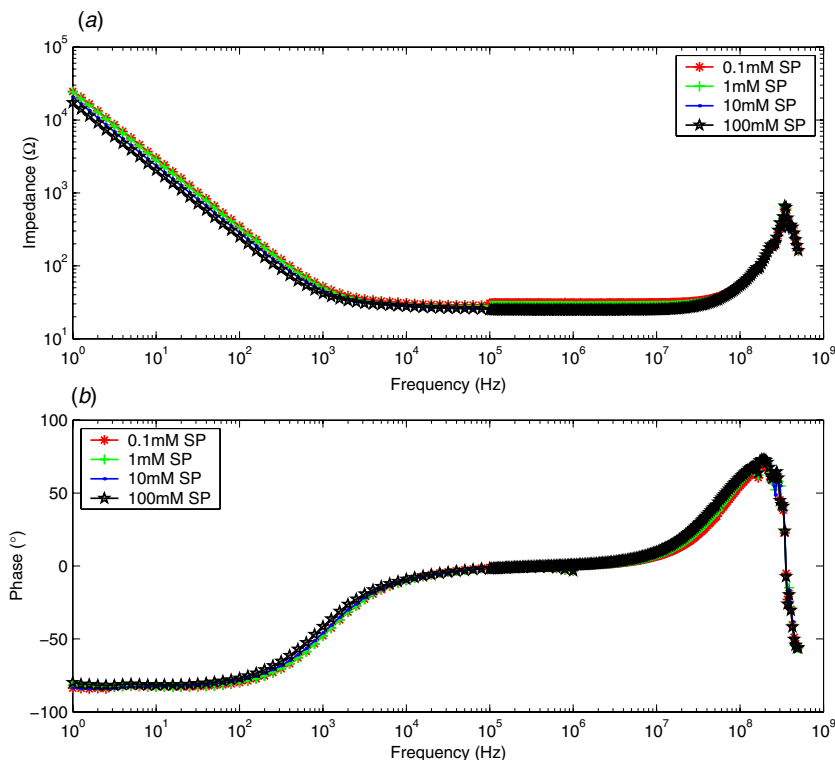


**Figure 4.** Impedance spectra measured at 10 mV applied  $V_{rms}$  for different concentrations of SP: (a) impedance magnitude plot and (b) impedance phase plot as a function of frequency for the blank sensor.

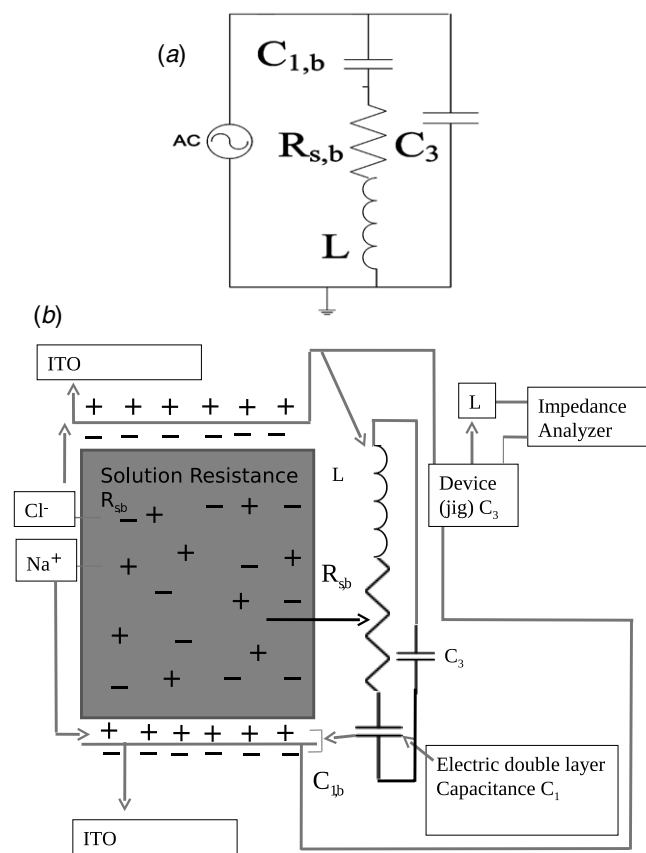


**Figure 5.** (a) Equivalent circuit of the blank sensor and (b) its corresponding designation within the sensor.

**Table 1.** Electrical element values in the equivalent circuit of the blank sensor shown in figure 5(a) as a function of SP concentration as obtained from the fitting of the impedance and phase spectra.

conc. (mM)	$C_{1,b}$ ( $\mu$ F)	$C_3$ (pF)	$R_3$ ( $\Omega$ )	$L$ (nH)
$\approx 0.001$	$4.38 \pm 0.62$	$3.5 \pm 0.0$	$397 \pm 21$	$72.5 \pm 2.5$
0.1	$4.35 \pm 0.80$	$3.5 \pm 0.0$	$40.8 \pm 5.0$	$80.8 \pm 16.1$
1	$4.88 \pm 0.76$	$3.5 \pm 0.0$	$36.2 \pm 4.5$	$85.0 \pm 15.3$
10	$5.84 \pm 1.04$	$3.5 \pm 0.0$	$32.7 \pm 3.6$	$85.0 \pm 15.3$
100	$6.97 \pm 1.20$	$3.5 \pm 0.0$	$28.2 \pm 1.7$	$83.3 \pm 15.5$

The values of the elements of the equivalent circuit for the blank sensor as a function of SP concentrations are presented in figure 7. At frequencies below 1 kHz, impedance decreases with increasing frequency. The current flow passes mostly through the double layer,  $C_{1,b}$ , which is formed at the solution/electrode interface and hence  $C_{1,b}$  dominates in this frequency range. Charge density in the double layer increases with the increase of concentration and hence capacitance ( $C_{1,b}$ ) increases. Debye lengths calculated for various concentrations (0.1, 1, 10, 100 mM) are 30.4, 9.61, 3.04 and 0.961 nm respectively. This suggests that  $C_{1,b}$  is not only related to the thickness of double layer but also to the area of the electrode. With increasing salt concentration, the resistance  $R_{s,b}$  decreases as expected based on bulk ionic strength effects. The flat impedance from 1 kHz and 100 MHz is indicative of resistive  $R_{s,b}$  dominance in the circuit, where the impedance of the solution is independent of the driving frequency. The increase of ion concentration increases the conductivity, i.e.

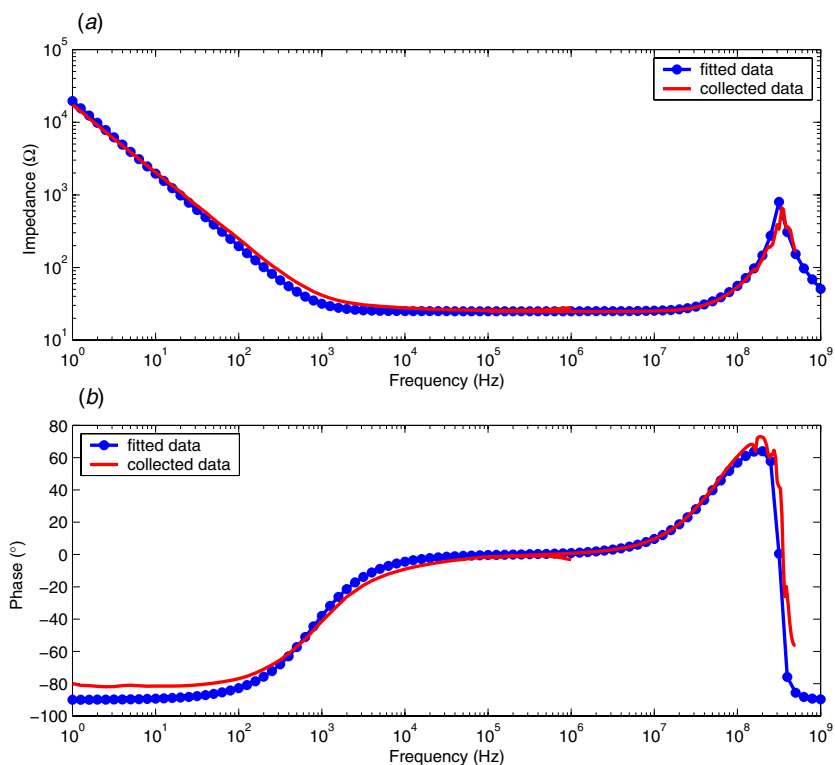


**Figure 6.** (a) Measured and fitted impedance magnitude plot and (b) measured and fitted impedance phase plot as a function of frequency for the blank sensor.

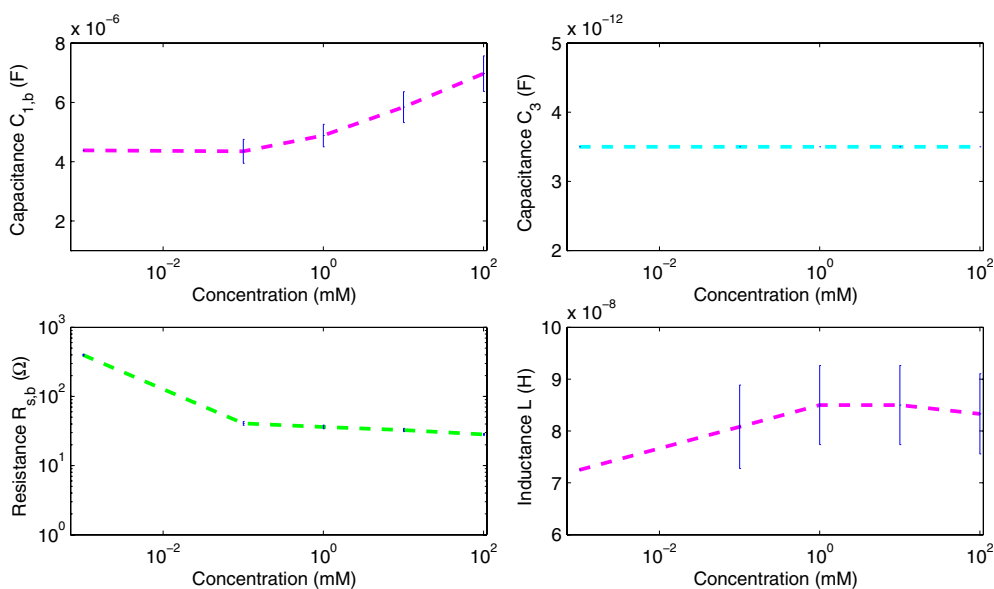


**Figure 7.** The values of the elements of the equivalent circuit for the blank sensor as a function of SP concentrations.

$R_{s,b}$  decreases with the increase in concentration. In the frequency range from 100 and 300 MHz, the impedance is dominated by the inductance  $L$ . The inductance is due to electrical leads and the measurement instrumentation.  $L$  is independent of ion concentration and no change in impedance spectra in that frequency range is observed. At frequencies above 300 MHz, device capacitance  $C_3$  dominates. Since  $C_3$  is due to the parallel plate configuration of the sensor, it is

also independent of ion concentration. Hence, no change in impedance spectra is observed, as expected.

### 3.2. VANS sensor

Figures 8(a) and (b) are frequency-dependent impedance and phase spectra of the VANS sensor, respectively, for various SP concentrations (0.1, 1, 10 and 100 mM). Detailed

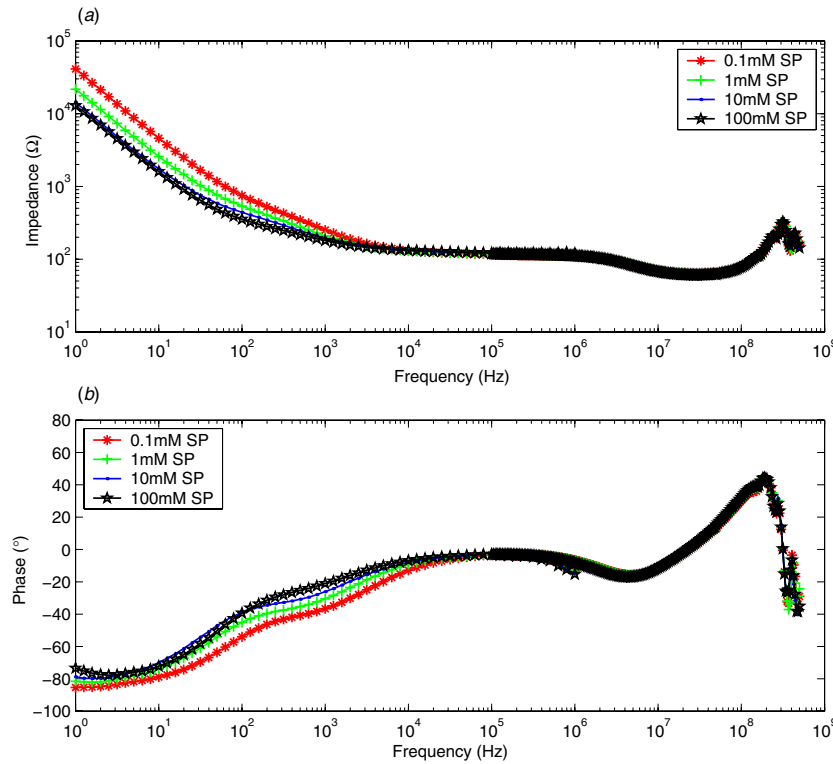


**Figure 8.** Impedance spectra measured at 10 mV applied  $V_{rms}$  for different concentrations of SP. (a) Impedance magnitude plot and (b) impedance phase plot as a function of frequency for the VANS sensor.

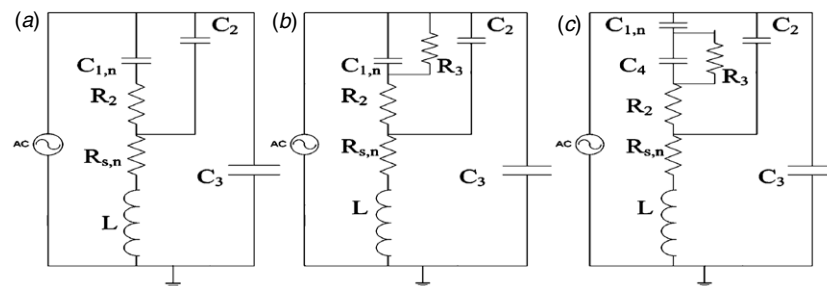


**Figure 9.** (a), (b) and (c) equivalent circuits for the VANS sensor.

examination reveals that below 9 kHz the impedance decreases with increasing SP concentrations, which is to be expected. However, above 9 kHz no significant change in impedance is observed.

Three equivalent circuits are proposed to model the characteristics of the VANS impedance and phase spectra [30–32]. The three equivalent circuits are displayed in figure 9. Note that there is no unique equivalent circuit, so one must construct an equivalent circuit such that the elements correspond to the physical attributes of the VANS sensor. The circuit in figure 9(a) is equivalent to the circuit for the blank sensor, shown in figure 5(a), with the addition of a second capacitor  $C_2$  and a second resistor  $R_2$ . In this circuit, the VANS have the effect of adding capacitance in parallel and resistance in series with the blank sensor. The circuit in figure 9(b) adds a slightly higher level of complexity to the circuit in figure 9(a) with the introduction of a resistance  $R_3$ . Finally, the circuit in figure 9(c) is the most complex with the

addition of a second capacitor  $C_4$ . The physical justification of the elements in each circuit follows.

The equivalent circuit in figure 9(a) did not satisfactorily reproduce the impedance characteristics in figure 8. In particular, it failed to account for the resistive behavior in the 10–100 Hz range. Assuming that VANS inhibit ion diffusion due to the physical constriction of their flow to the base of the electrode, a resistor  $R_3$  is added in parallel with  $C_{1,n}$ , as shown in figure 9(b). The addition of  $R_3$  to the equivalent circuit also failed to reproduce the impedance spectra in the 10–100 Hz frequency range. We propose that an additional electric double layer  $C_4$  forms on the VANS. With the addition of  $C_4$  in series with  $C_{1,n}$  shown in figure 9(c), we obtain the best fits to the experimental spectra. A physical representation of the elements of the model equivalent circuit in figure 9(c) as they pertain to the VANS sensor is outlined in figure 10.

**Table 2.** Average values of the circuit elements in the equivalent circuit shown in figure 9(c) obtained from fitting the experimental impedance spectra as a function of SP concentration for the VANS sensor.

conc. (mM)	$C_{1,n}$ ( $\mu$ F)	$C_2$ (nF)	$C_3$ (pF)	$C_4$ ( $\mu$ F)	$R_{s,n}$ ( $\Omega$ )	$R_2$ ( $\Omega$ )	$R_3$ (k $\Omega$ )	$L$ (nH)
$\approx 0.001$	$1.15 \pm 0.01$	$0.05 \pm 0.00$	$3.5 \pm 0.0$	$4.55 \pm 1.05$	$54 \pm 6$	$163 \pm 37$	$7.6 \pm 1.1$	$75 \pm 5$
0.1	$5.48 \pm 0.54$	$0.32 \pm 0.11$	$3.5 \pm 0.0$	$0.56 \pm 0.06$	$55.3 \pm 3.5$	$32.9 \pm 4.8$	$1.44 \pm 0.40$	$68.3 \pm 1.7$
1	$6.14 \pm 0.51$	$0.32 \pm 0.11$	$3.5 \pm 0.0$	$0.64 \pm 0.07$	$55.1 \pm 3.5$	$32.6 \pm 4.8$	$1.05 \pm 0.25$	$68.3 \pm 1.7$
10	$6.80 \pm 0.59$	$0.33 \pm 0.11$	$3.5 \pm 0.0$	$0.71 \pm 0.07$	$55.1 \pm 3.8$	$32.6 \pm 4.7$	$0.86 \pm 0.20$	$68.3 \pm 1.7$
100	$7.20 \pm 0.59$	$0.33 \pm 0.11$	$3.5 \pm 0.0$	$0.86 \pm 0.11$	$54.7 \pm 3.8$	$32.2 \pm 4.8$	$0.70 \pm 0.17$	$68.3 \pm 1.7$

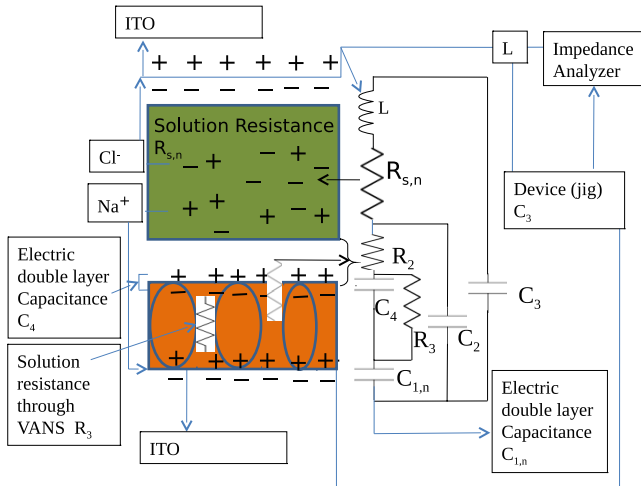


**Figure 10.** Schematic representation of the circuit elements within the sensor.

Figures 11(a) and (b) show the measured and fitted impedance and phase spectra for a 100 mM concentration of

the SP solution, which demonstrates good agreement between the circuit model and the experimental data. However, at frequencies below 100 Hz the phase of the equivalent circuit reaches the ideal value of  $-90^\circ$ , while the VANS sensor only reaches  $-70^\circ$ , which is less than  $-80^\circ$  for the blank sensor. This is likely due to the overly simplistic nature of the equivalent circuit and the more complex ionic motion that occurs at low frequencies. The impedance spectra for other concentrations (0.1, 1 and 10 mM) were fitted with the equivalent circuit in figure 9(c), where the fits are of equally good quality. We analyzed nine individual VANS sensors with deionized water and the four SP concentrations with the equivalent circuit in figure 9(c). Table 2 demonstrates a summary of the average values of the elements of the nine VANS sensors. Note that the lowest concentration of 0.001 mM refers to deionized water.

The standard deviations of the elements in table 2 do not vary more than 30% from sensor to sensor, but are typically less than 10%. When taken in conjunction with their assignment to the VANS mat, one can speculate that variations in the porosity may positively or negatively affect ionic diffusion

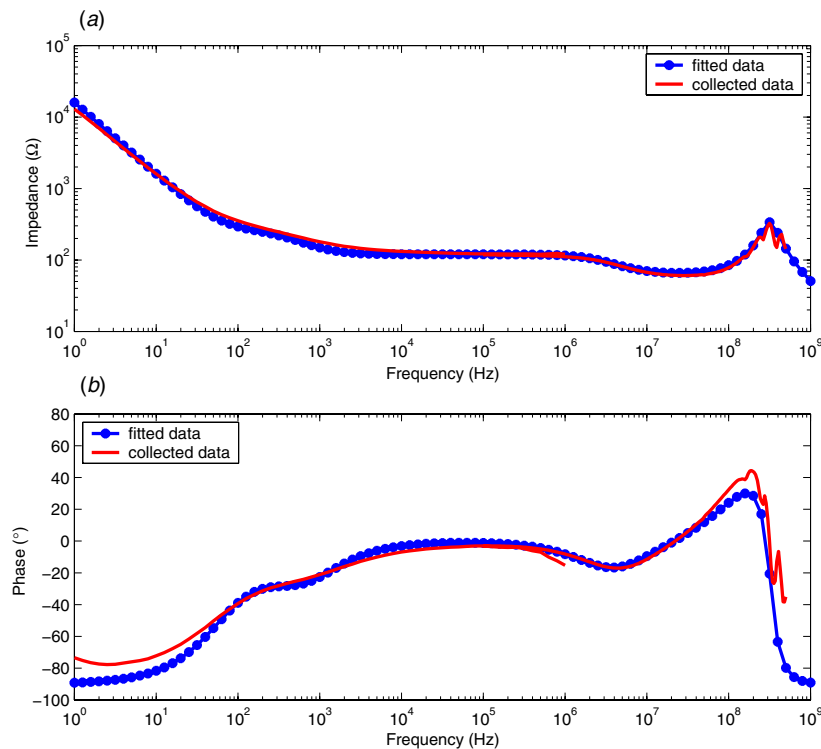


**Figure 11.** (a) Measured and fitted impedance magnitude plot and (b) measured and fitted impedance phase plot as a function of frequency for the VANS sensor.

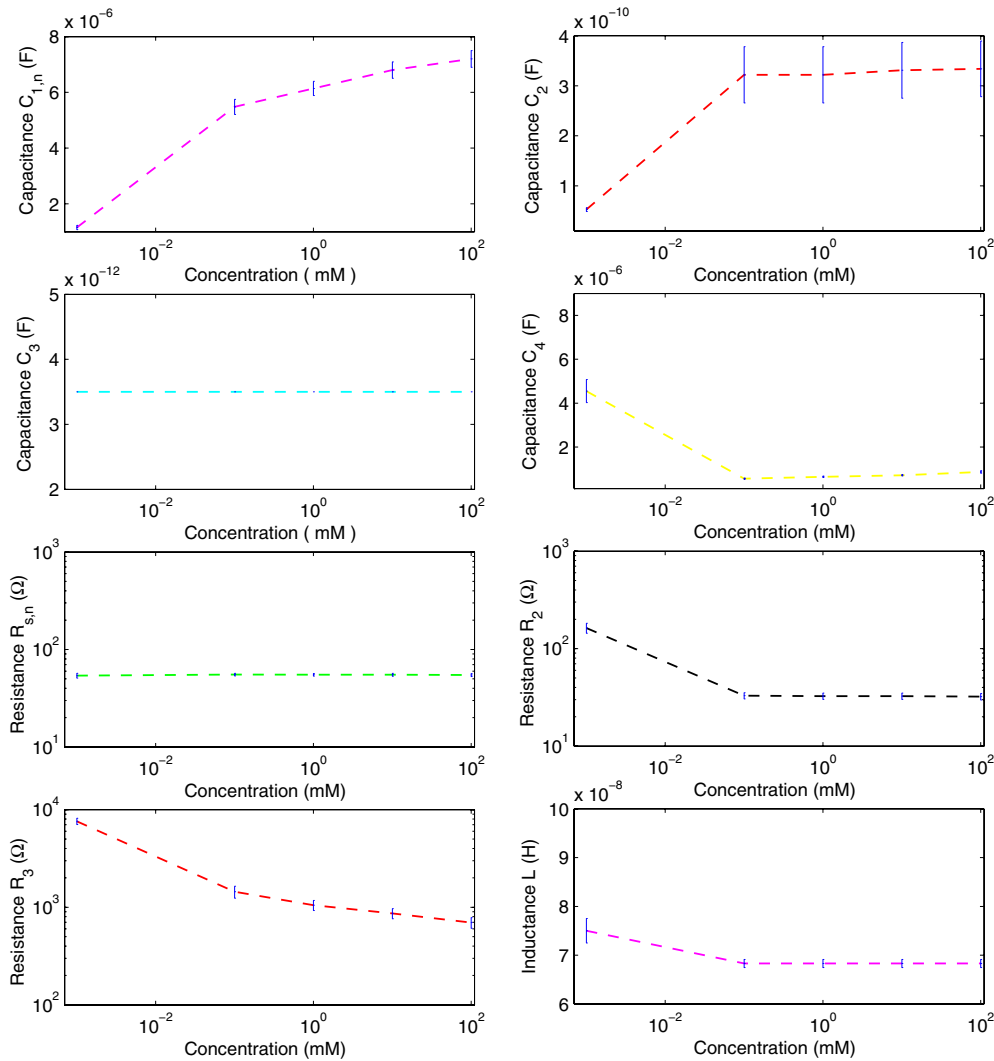


**Figure 12.** The values of the elements of the equivalent circuit for the VANS sensor as a function of SP concentration.

within the mat. The concentration-dependent values of the elements of the equivalent circuit shown in figure 9(c) are presented in figure 12.  $C_{1,n}$  corresponds to the solution–electrode interface and dominates the circuit below 100 Hz. As the concentration of solution increases, charge density in the double layer  $C_{1,n}$  increases. Hence, the capacitance  $C_{1,n}$  increases. An additional double layer  $C_4$  is formed at the solution–VANS interface.  $R_3$  and  $C_4$  influences are predominant in the frequency range from 100 Hz and 10 kHz.  $R_3$  decreases with increasing ion concentration of the solution, which is to be expected.  $C_4$  is an order of magnitude less than  $C_{1,n}$ . This implies that either a high voltage is required to accumulate ions at the solution–VANS interface relative to the planar surface of the electrode or that the porosity of the interface, which has a reduced surface area, limits the accumulation of ions. It is the opinion of the authors that the latter is true. A slight increase in the values of  $C_4$  with the increase of solution concentration indicates that the additional ions accumulated at the double layer  $C_4$  but not to the same extent as at the double layer  $C_{1,n}$ . The influence of  $R_{s,n}$  is predominantly in the frequency range of 10 kHz–10 MHz, where  $R_{s,n}$  is independent of the driving frequency

and concentration of solution.  $C_2$  has the greatest influence on the VANS sensor in the frequency range of 2–10 MHz and is independent of the ionic concentration of the solution. However,  $C_2$  has a large standard deviation of  $\approx 30\%$ . This might be due to variations in the thickness of VANS mat from sensor to sensor. The influence of  $R_2$  is primarily in the frequency range of 10–100 MHz and is independent of the solution concentration.  $R_2$  is attributed to the transport barrier of the ions in and out of the VANS mat. This barrier is the VANS electric double layer,  $C_4$ , which impedes the diffusion of the ions from the VANS-free solution to the solution within the VANS region. The absence of response of  $R_2$  to changes in the ionic concentration suggests that the electric double layer at the solution–VANS interface is not affected by increasing ion concentrations, where the VANS morphology limits ion loading. This is consistent with the independence of  $C_4$  to changes in the ionic concentration of the solution, as well as our assignment of  $C_4$  to the solution–VANS interface. However, this does not imply that the VANS electric double layer below this boundary remains unchanged. In fact, the examination of table 2 shows that  $C_{1,n}$  does indeed increase with ionic concentration. One might speculate that  $R_3$  arises from the

physical size of the channels between neighboring VANS. The large standard deviation  $\approx 25\%$  of  $R_3$  suggest that there are large variations in either the size of the VANS structures, the porosity of the mat or the packing density of the VANS from sensor to sensor, or all of the above. The inductance  $L$  dominates in the frequency range from 100–300 MHz, and as in the blank sensor,  $L$  is attributed to the test apparatus and electrical leads.  $C_3$  dominates at frequencies above 300 MHz and is again due to the parallel plate configuration of the sensor.

### 3.3. Comparison of the VANS sensor against the blank sensor

As mentioned in section 3.1 and 3.2 above, below 60 Hz the impedance spectra for blank sensors decrease with an increase in salt concentration, whereas spectra of the VANS sensors decrease with increasing salt concentration below 9 kHz. At frequencies below 100 Hz, there is a 28% decrease in impedance of the blank sensors with increasing concentrations from 0.1 to 100 mM, which is significantly lower than the 68% decrease in impedance of the VANS sensors. The impedance spectra for the blank sensors have been fitted using a simple equivalent circuit consisting of circuit elements  $C_{1,b}$ ,  $R_{s,b}$ ,  $C_3$  and  $L$ , where  $C_{1,b}$  and  $R_{s,b}$  are concentration dependent. This is consistent with previously reported impedance spectroscopy of similar device geometries. The presence of the VANS significantly modifies the ionic transport within the device. Therefore, the impedance spectra of the VANS sensors are significantly more complicated relative to the blank sensor and require additional elements ( $C_4$ ,  $R_2$ ,  $R_3$  and  $C_2$ ). The circuit elements  $C_2$ ,  $R_{s,n}$  and  $R_2$  of the VANS sensor are essentially constant over the entire range of SP concentrations. However,  $C_4$  and  $R_3$  are concentration-dependent circuit elements and are very sensitive to the change of SP concentration, particularly in the frequency range of 100 Hz to 9 kHz. The complexity introduced by the VANS enhances sensitivity at frequencies below 9 kHz. As the SP concentration increases from 0.1 to 100 mM, the percentage change in the slope of the VANS signal is 74% in the frequency range of 100 Hz to 9 kHz compared to the change of 28% in the blank sensor. One can deduce that the future development of biofunctionalized VANS sensors will outperform blanks or similar planar sensors. In terms of VANS sensor operation, the most relevant frequency range is from 1 Hz to 10 MHz. Our expectation is that the addition of biological materials to the VANS will change the fitted values of these equivalent circuit elements (especially those most affected by salt concentrations) or more likely provide spectra that require the addition of circuit elements. By focusing on the elements impacted by the biological material, the objective will be to tune the sensor characteristics to provide the greatest sensitivity and discrimination.

## 4. Conclusions

This study demonstrated the successful characterization of a VANS sensor in an ionic solution using AC impedance spectroscopy. A more complex equivalent circuit is required to fit impedance spectra for a VANS sensor compared to a blank

sensor. The additional circuit elements, electric double layer capacitance  $C_4$ , capacitance  $C_2$ , the solution–VANS interface resistance  $R_2$  and the solution resistance through the VANS  $R_3$ , suggest that VANS behave not only like a resistive layer but also as a capacitive network. Based on the extracted numerical values of the equivalent circuit elements of the blank sensor given in table 1, one can see that the most responsive elements to changes in the ion concentrations are  $C_{1,b}$  and  $R_{s,b}$ . However, for the VANS sensor,  $C_{1,n}$ ,  $C_4$  and  $R_3$  are the most sensitive elements of the equivalent circuit. This study has demonstrated that sensors constructed with VANS are significantly more sensitive to changes in ion concentrations of the solution relative to the flat and smooth blank sensors. Furthermore, this work lays down the foundation for the next phase of VANS-based biosensors.

## Acknowledgments

The authors are indebted to support from the Biological Applications of Nanotechnology (BANTech) program at the University of Idaho, and the support of the NSF-Idaho EPSCoR Program and by the National Science Foundation under award no. EPS-00447689.

## References

- [1] Kissinger P T 2005 *Biosens. Bioelectron.* **20** 2512
- [2] Murphy L 2006 *Curr. Opin. Chem. Biol.* **10** 177
- [3] Bogue R 2005 *Sensor Rev.* **25** 180
- [4] Jianrong C, Yuqing M, Nongyue H, Xiaohua W and Sijiao L 2004 *Biotechnol. Adv.* **22** 505
- [5] Beaux M F II, McIlroy D N and Gustin K E 2008 *Expert Opin.* **5** 725
- [6] Adili A, Crowe S, Beaux M F II, Cantrell T, Shapiro P J, McIlroy D N and Gustin K E 2008 *Nanotoxicology* **2** 1
- [7] Zhang H F, Wang C M, Buck E C and Wang L S 2003 *Nano Lett.* **3** 577
- [8] Wang L, Major D, Paga P, Zhang D, Norton M G and McIlroy D N 2006 *Nanotechnology* **17** S298
- [9] McIlroy D N, Zhang D and Kranov Y 2001 *Appl. Phys. Lett.* **79** 1540
- [10] Corti G, Wang L, Major D, Branen J, Jabal J, Branen L, Nagler J, Aston E, Norton G and McIlroy D 2007 *Mater. Res. Soc. Proc. MRS* **1010-V05-03**
- [11] McIlroy D N, Alkhateeb A, Zhang D, Aston D E, Marcy A C and Norton M G 2004 *J. Phys.: Condens. Matter* **16** R415
- [12] Macdonald D D 2006 *Electrochim. Acta* **51** 1376
- [13] Katz E and Willner I 2003 *Electroanalysis* **15** 913
- [14] Macdonald J R 1992 *Ann. Biomed. Eng.* **20** 289
- [15] Marcus P and Mansfeld F 2006 *Analytical Methods in Corrosion Science and Newline Engineering* (Boca Raton, FL: CRC Press) p 463
- [16] Senturia S 2001 *Microsystem Design* (New York: Kluwer) p 73
- [17] Norton G and McIlroy D US Patent Application 11/993452 filed
- [18] Hillebrandt H, Weigand G, Tanaka M and Sackmann E 1999 *Langmuir* **15** 8451
- [19] Daniels J S and Pourmand N 2007 *Electroanalysis* **19** 1239
- [20] Rodríguez M C, Kawde A N and Wang J 2005 *Chem. Commun.* **34** 4267
- [21] Hillebrandt H and Tanaka M 2000 *J. Phys. Chem. B* **105** 4270
- [22] Yang L, Li Y and Erf G F 2004 *Anal. Chem.* **76** 1107
- [23] Yang L and Li Y 2005 *Biosens. Bioelectron.* **20** 1407

- [24] Halme J, Toivola M, Tolvanen A and Lund P 2006 *Solar Energy Mater. Solar Cells* **90** 872
- [25] Pänke O, Balkenhohl T, Kafka J, Schafer D and Lisdat F 2008 *Adv. Biochem. Eng./Biotechnol.* **109** 195
- [26] Kim C O, Hong S Y, Kim M, Park S M and Park J W 2004 *J. Colloid Interface Sci.* **277** 499
- [27] Kötz R and Carlen M 2000 *Electrochim. Acta* **45** 2483
- [28] Qu D 2002 *J. Power Sources* **109** 403
- [29] Janek R P and Fawcett W R 1998 *Langmuir* **14** 3011
- [30] Li C Z, Liu Y and Luong J H T 2005 *Anal. Chem.* **77** 478
- [31] Attar M M, Naderi R and Moayed M H 2005 *Mater. Corros.* **56** 325
- [32] Sweitlow A, Skoog M and Johansson G 1992 *Electroanalysis* **4** 921